Coherent electron flow from a double slit with slit widths in the quantum conductance regime

2006 J. Phys.: Condens. Matter 18 11103

(http://iopscience.iop.org/0953-8984/18/49/005)

INSTITUTE OF PHYSICS PUBLISHING JOURNAL OF PHYSICS: CONDENSED MATTER

J. Phys.: Condens. Matter **18** (2006) 11103–11119 doi:10.1088/0953-8984/18/49/005

Coherent electron flow from a double slit with slit widths in the quantum conductance regime

Lebo Zhang and H Q Xu

School of Physics and Optoelectronic Technology, Dalian University of Technology, Dalian 116024, People's Republic of China
and
Division of Solid State Physics, Lund University, Box 118, S-22100 Lund, Sweden

E-mail: Hongqi.Xu@ftf.lth.se

Received 8 August 2006, in final form 4 November 2006
Published 22 November 2006
Online at stacks.iop.org/JPhysCM/18/11103

Abstract

We report on a theoretical study of the quantum interference behaviour of electron flow from a double-slit device made from a semiconductor two-dimensional electron gas (2DEG) system with the slit widths in the quantum conductance regime. The device consists of a double slit and a single slit in a configuration where the single slit is placed on the source side of the double slit. The wavefunctions of electrons passing through the double-slit structure are calculated on the basis of a scattering matrix method. It is found that including a single slit between the double slit and the source contact in the device is essential for the observation of interference fringes of electron flow in a double-slit experiment with a 2DEG. When only the lowest mode is open for conduction in the individual slits, the interference patterns of electron flow from the double slit resemble the results of a conventional Young's double-slit experiment well. When several modes are open for conduction in the individual slits, the interference patterns of electron flow from the double slit are dominated by the interference of electrons flowing through the highest index open modes in the slits. As a result of the existence of multiple-lobe structures in electron flow from these high index open modes, these interference patterns, in general, show rather complex structures. We also discuss the characteristics of interference patterns in the near- and far-field regimes and the dependence of the fringe spacing on the slit distance in the double slit.

(Some figures in this article are in colour only in the electronic version)

1. Introduction

One of the most beautiful experiments in physics is the interference of electrons in a Young's double slit [1–3]. In such an experiment, single electrons interfere with themselves to produce the famous interference pattern known in the double-slit experiment for light [2, 3]. It was thus

confirmed that electrons possess wave-like properties. For a free electron, the associated wave has a wavelength related to the magnitude of the momentum, p, of the electron by $\lambda = h/p$. In analogy to the optical Young's experiment, the interference pattern of electrons in the double-slit experiment can be described by a simple formula derivable by considering that the electron wavefronts in the two slits behave like two stripes of an infinite number of point sources with the same wave intensity and phase and, thus, the electron wave has a uniform front on leaving from the two slits. Here, the quantum confinement imposed by the slit boundaries on the electron wave is assumed to have no effect on the interference phenomenon. This is a good assumption for the reported electron double-slit experiments [1–3], in which the lateral width of the slits is several orders of magnitude larger than the wavelength of the electrons. However, experiments on the electron transport through quantum point contacts made from semiconductor heterostructures have shown that the electron wave propagates through a narrow opening via certain lateral quantum states and thus has a spatially nonuniform profile of the wave intensity when emitting from the opening [4–6]. Does this quantum effect give observable new interference phenomena in double-slit experiments for electrons? This essential question would also be asked in quantum optics experiments.

Experimentally, the problem could be studied by imaging the wavefunctions of electrons flowing from a double slit defined in a two-dimensional electron gas (2DEG) system made with a semiconductor heterostructure. A variety of scanning probe microscope (SPM) techniques have been developed for imaging electron wavefunctions in recent years [4–19]. These techniques have been successfully applied to image, e.g., coherent electron flow from a quantum point contact [4–7], electron wavefunctions in carbon nanotubes [10, 11], single-electron charge states in nanotube quantum dots [12], localized electron states and resonances in the quantum Hall regime [13, 18], scarred wavefunctions in quantum billiards [16], and fine interference fringes in an imaging electron interferometer [19]. However, no imaging experiment on electron flow from a double-slit structure made from a 2DEG has been reported. It should be noted that an observation of electron interference in a double slit made from a semiconductor heterostructure was recently reported [20]. However, the electron flow was made in this experiment along the vertical direction and, therefore, no electron flow pattern could be imaged.

In this work, we present a theoretical study of the effects of modal structures on electron interference by quantum-mechanical simulation of coherent electron flow from a double-slit structure made from a 2DEG system. The device is assumed to consist of a double slit and a single slit with the single slit being placed on the electron source side of the double slit. The single and double slits are connected, respectively, with the electron source and collector contacts by two wide 2DEG regions. The wavefunctions of electrons flowing through the device are calculated. To simulate a double-slit experiment made in a 2DEG, a model device with sufficiently large dimensions needs to be assumed (e.g., $\sim$5 μm was assumed for the lateral size of the device studied in this work). Thus, the calculations are numerically very demanding. In this work, we carry out these wavefunction calculations with the use of a scattering matrix method [21, 22]. We find that introducing a single slit in front of the double slit is essential for the observation of a fine interference pattern of electron flow from the double slit. We also find that when only the lowest mode is open for conduction in the individual slits, the interference patterns of electron flow from the double slit resemble the results of a conventional Young's double-slit experiment well. When several modes are open for conduction in the individual slits, the interference patterns of electron flow from the double slit are dominated by the interference of electrons flowing through the highest index open modes in the slits and, in general, show rather complex structures, as a result of the existence of multi-lobe structures in the electron flow from these high index open modes.

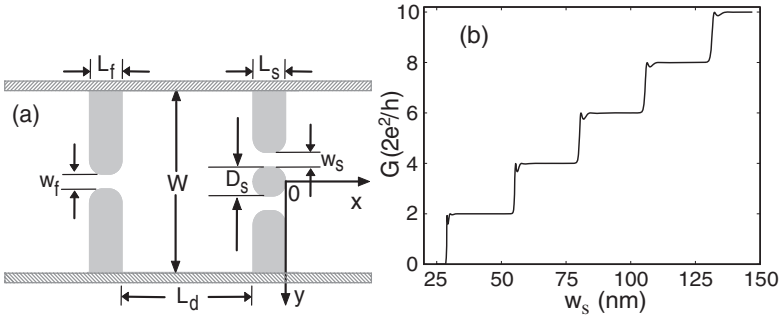

Figure 1. (a) Schematic diagram of the electron double-slit device studied in this work. The device consists of a double slit and a single slit. The single slit is placed on the source contact side of the double slit in order to create a coherent source of electrons with similar incident conditions. (b) Calculated conductance of the double slit (a structure without the presence of the single slit in (a)) as a function of the slit width w_s. The device parameters used in the calculation are lateral width of the 2DEG regions $W = 5\ \mu$m, slit length $L_s = 800$ nm, slit distance $D_s = 500$ nm, radius of quarter-circles in slit corners $R_s = 200$ nm, and electron Fermi energy $E_F = 8.6$ meV.

The rest of the paper is organized as follows. In section 2, the model and scattering matrix method employed in this work are briefly described. In section 3, we present and discuss the calculated interference patterns of electron flow from the double-slit device with different slit widths and thus different numbers of open modes in the slits. Here we will also discuss the role of the single slit placed in front of the double slit in the Young's interference experiments for electrons. Finally, the paper is summarized and concluded in section 4.

2. Model and scattering matrix method

The system under consideration is assumed to be made from a 2DEG defined in a semiconductor heterostructure with growth direction along the z axis. It is further assumed that the 2DEG is bounded and has a width W in the transverse y direction, and the electron transport takes place along the longitudinal x direction. In the calculations, the width W is chosen to be large enough that the transverse boundaries have negligible effects on the results of calculations. The structure of the electron double-slit system considered, made in the 2DEG, is schematically shown in figure 1(a), where the double slit is modelled by two identical slits in parallel. It should be noted that in an electron double-slit Young's experiment, it is important that the electrons which pass through the double slit are coherent and have the same initial injection condition. In practice, this can approximately be realized by sending electrons toward the double slit from a single point-like source. In the present work, we model this situation by placing a single slit in front of the double slit. We will show that introducing such a single slit in a position between the electron source contact and the double slit is essential for an electron double-slit experiment with a 2DEG. This is because there is no coherence between electrons emitted from the source contact and the interference pattern will be smoothed away by an averaging of the contributions from individual electrons injected from the source contact with different initial conditions.

The Schrödinger equation of an electron in the system considered with energy ε can be written, under the effective mass approximation, as

$$\left\{-\frac{\hbar^2}{2m^*}\left[\frac{\partial^2}{\partial x^2}+\frac{\partial^2}{\partial y^2}\right]+V_c(y)+V_E(x,y)\right\}\Psi(x,y)=\varepsilon\Psi(x,y), \tag{1}$$

where $V_c(y)$ describes the transverse confining potential of the wide 2DEG and $V_E(x, y)$ the potential which defines the double slit and the single slit. In the study of the electron flow problem in the system, the Schrödinger equation needs to be solved at a given energy ε for all possible eigensolutions including both propagating and evanescent states. This clearly is a numerically demanding task. Here we will overcome the difficulty by employing a scattering matrix method [21, 22].

In the scattering matrix method, the Schrödinger equation is solved by discretizing the system along the x direction into a large number N of transverse stripes, such that the potential $V_E(x, y)$ in each stripe can be considered to be independent of the coordinate x and can therefore be approximately written as $V_E^i(y)$. Thus the wavefunction of an electron with energy ε in the ith stripe can be written as

$$\Psi^i(x, y) = \sum_n \phi_n(y) \sum_\alpha d^i_{n\alpha}[a^i_\alpha e^{ik^i_\alpha(x-x^i_0)} + b^i_\alpha e^{-ik^i_\alpha(x-x^i_0)}], \tag{2}$$

where $\phi_n(y) = \sqrt{\frac{2}{W}} \sin \frac{n\pi y}{W}$ are the eigenstates of the wide 2DEGs with width W, x^i_0 is the reference point for the ith stripe along the x direction and can be chosen at the left edge of the ith stripe, and $k^i_\alpha = [2m^*(\varepsilon - E^i_\alpha)/\hbar^2]^{1/2}$. The expansion coefficients, $d^i_{n\alpha}$, can be obtained by searching for eigenvalues E_α from the system,

$$\sum_m \left[(\varepsilon_m - E^i_\alpha)\,\delta_{nm} + \langle\phi_n(y)|V^i_E(y)|\phi_m(y)\rangle\right] d^i_{m\alpha} = 0, \qquad n = 1, 2, 3, \ldots, \tag{3}$$

where $\varepsilon_m = \frac{\hbar^2}{2m^*}(\frac{\pi m}{W})^2$. The coefficients, $\{a^i_\alpha\}$ and $\{b^i_\alpha\}$, in equation (2) are determined by the boundary condition of the problem. For simplicity, we will in the following denote the coefficients, $\{a^i_\alpha\}$ and $\{b^i_\alpha\}$, by vectors $\mathbf{A}^i$ and $\mathbf{B}^i$. In the present work, these coefficients are calculated by employing scattering matrices [21, 22] as follows. The incoming states, $\mathbf{A}^L$ and $\mathbf{B}^R$, and the outgoing states, $\mathbf{A}^R$ and $\mathbf{B}^L$, in the left (L) and right (R) wide 2DEG regions are related by the scattering matrix $\mathbf{S}(L, R)$,

$$\begin{bmatrix} \mathbf{A}^R \\ \mathbf{B}^L \end{bmatrix} = \begin{bmatrix} \mathbf{S}_{11}(L, R) & \mathbf{S}_{12}(L, R) \\ \mathbf{S}_{21}(L, R) & \mathbf{S}_{22}(L, R) \end{bmatrix} \begin{bmatrix} \mathbf{A}^L \\ \mathbf{B}^R \end{bmatrix}. \tag{4}$$

The coefficient vectors, $\mathbf{A}^i$ and $\mathbf{B}^i$, in the ith stripe, can also be related to the coefficient vectors of the incoming waves in the two 2DEG regions, $\mathbf{A}^L$ and $\mathbf{B}^R$. To show this we employ the scattering matrices $\mathbf{S}(L, i)$ and $\mathbf{S}(i, R)$ and write

$$\begin{aligned} \begin{bmatrix} \mathbf{A}^i \\ \mathbf{B}^L \end{bmatrix} &= \begin{bmatrix} \mathbf{S}_{11}(L, i) & \mathbf{S}_{12}(L, i) \\ \mathbf{S}_{21}(L, i) & \mathbf{S}_{22}(L, i) \end{bmatrix} \begin{bmatrix} \mathbf{A}^L \\ \mathbf{B}^i \end{bmatrix}, \\ \begin{bmatrix} \mathbf{A}^R \\ \mathbf{B}^i \end{bmatrix} &= \begin{bmatrix} \mathbf{S}_{11}(i, R) & \mathbf{S}_{12}(i, R) \\ \mathbf{S}_{21}(i, R) & \mathbf{S}_{22}(i, R) \end{bmatrix} \begin{bmatrix} \mathbf{A}^i \\ \mathbf{B}^R \end{bmatrix}. \end{aligned} \tag{5}$$

The above equations express the coupling of the electron wavefunction in the left 2DEG region with the wavefunction in the ith stripe and the coupling of the wavefunction in the ith stripe with that in the right 2DEG region, respectively. Solving for $\mathbf{A}^i$ and $\mathbf{B}^i$ from equation (5) gives

$$\begin{aligned} \mathbf{A}^i &= [1 - \mathbf{S}_{12}(L, i)\mathbf{S}_{21}(i, R)]^{-1}[\mathbf{S}_{11}(L, i)\mathbf{A}^L + \mathbf{S}_{12}(L, i)\mathbf{S}_{22}(i, R)\mathbf{B}^R], \\ \mathbf{B}^i &= [1 - \mathbf{S}_{21}(i, R)\mathbf{S}_{12}(L, i)]^{-1}[\mathbf{S}_{21}(i, R)\mathbf{S}_{11}(L, i)\mathbf{A}^L + \mathbf{S}_{22}(i, R)\mathbf{B}^R]. \end{aligned} \tag{6}$$

Since the coefficient vectors $\mathbf{A}^L$ and $\mathbf{B}^R$ are known from the boundary condition, equations (4) and (6) imply that once the scattering matrices, $\mathbf{S}(L, i)$, $\mathbf{S}(i, R)$ and $\mathbf{S}(L, R)$, are found, all the coefficient vectors, $\mathbf{A}^i$ and $\mathbf{B}^i$, as well as $\mathbf{A}^R$ and $\mathbf{B}^L$, required for a complete description of the wavefunction of the electron incident from the left can be obtained. With the help of the transfer matrices derived in [23] for such a planar system, all these scattering matrices can be calculated on the basis of an iterative method reported in [22].

For an electron injected into the system from the left in a state $\phi_m(y)\mathrm{e}^{\mathrm{i}k_m(x-x_0^L)}$ with energy ε, the wavefunction of the electron in the two wide 2DEG regions can be written as

$$\begin{aligned}\Psi^L(x,y) &= \phi_m(y)\mathrm{e}^{\mathrm{i}k_m(x-x_0^L)} + \sum_n \phi_n(y)\sum_\alpha d_{n\alpha}^L b_\alpha^L \mathrm{e}^{-\mathrm{i}k_\alpha^L(x-x_0^L)},\\ \Psi^R(x,y) &= \sum_n \phi_n(y)\sum_\alpha d_{n\alpha}^R a_\alpha^R \mathrm{e}^{\mathrm{i}k_\alpha^R(x-x_0^R)}.\end{aligned} \tag{7}$$

Thus, the boundary condition imposed on the wavefunction of the electron is

$$\begin{bmatrix}\mathbf{A}^L\\ \mathbf{B}^R\end{bmatrix} = \begin{bmatrix}\mathbf{I}_m\\ \mathbf{0}\end{bmatrix}, \tag{8}$$

where $\mathbf{I}_m$ is a unit vector with elements given by $(\mathbf{I}_m)_\alpha = \delta_{\alpha m}$. It is now straightforward to calculate the coefficient vectors $\mathbf{A}^i$ and $\mathbf{B}^i$, as well as $\mathbf{A}^R$ and $\mathbf{B}^L$, and thus the entire wavefunction, $\Psi_m(x,y)$, of the electron by inserting this boundary condition (equation (8)) into equations (4) and (6).

The electron density and current density, associated with this single electron, in stripe i are given by

$$\rho_m^i(x,y) = \Psi_m^{i*}(x,y)\Psi_m^i(x,y), \tag{9}$$

$$\mathbf{j}_m^i(x,y) = \frac{\mathrm{i}e\hbar}{2m^*}\left[\Psi_m^{i*}(x,y)\nabla\Psi_m^i(x,y) - \Psi_m^i(x,y)\nabla\Psi_m^{i*}(x,y)\right]. \tag{10}$$

In the linear response regime, the total electron density, $\rho^i(x,y)$, and the total current density, $\mathbf{j}^i(x,y)$, are obtained by summing all the contributions from electrons incident from the left at the Fermi energy E_F,

$$\rho^i(x,y) \sim \sum_{m=1}^M \rho_m^i(x,y)/k_m, \tag{11}$$

$$\mathbf{j}^i(x,y) \sim \sum_{m=1}^M \mathbf{j}_m^i(x,y)/k_m \tag{12}$$

where the wavevector $k_m = [2m^*(E_\mathrm{F}-\varepsilon_m)/\hbar^2]^{1/2}$ and M is the number of propagating modes, for which k_m is real, found in the left wide 2DEG region. Here we note that in an experiment, the electron transport properties (the conductance, charge density distribution, current flow, etc) are usually measured under a small voltage δV applied over the device. Thus, at sufficiently low temperature (zero temperature is assumed in this work), the measured transport quantities contain the contributions from all the injected electrons from a wide 2DEG region in the energy window $[E_\mathrm{F}, E_\mathrm{F}+\mathrm{e}|\delta V|]$. To make our calculations under a condition relevant to experiment, we need to take all these contributions into account. In the linear response regime, where the applied voltage is sufficiently small (i.e., $\delta V \to 0$), this can simply be achieved by multiplying the contribution from each individual open mode in the left wide 2DEG region with the local density of states (which is inversely proportional to the wavevector k_m) associated with that open mode and then summing over the results obtained for all the open modes at energy E_F.

The method presented above is formulated in a basis of infinite order and is exact. However, equation (3) needs to be solved numerically by truncating n and m at a high transverse level N. In the actual calculations we let N be as large as necessary to obtain a desired accuracy. Also the method is numerically stable and is efficient for solving for the electron flow patterns in devices with large dimensions and complicated structures. It should be noted that although it is straightforward to calculate the current densities from equations (10) and (12), we will in this work only present the results of calculations for the densities of electrons flowing from the double slit. This is because our calculated current densities and electron densities show

rather similar flow patterns in the system and also because it is the electron densities (electron wavefunctions) which are measured in most SPM experiments.

3. Results and discussion

In this work, we are interested in the interference patterns of electrons propagating through the double slit and, in particular, the effects of the modal structure formed in the narrow slits on the interference patterns. As is shown in figure 1(a), the two identical slits used to model the double slit have a width w_s and a length L_s, and are separated to a distance of D_s. The single slit has a width w_f and a length L_f and is placed in front of the double slit at a distance of L_d from the double slit. In order to reduce the effect of scattering from the sharp geometrical corners in the narrow opening slit region, each corner of the slits has been smoothed using a quarter of a circle with a radius of R_s. In this work, the effective mass of electrons is assumed to be $m^* = 0.067\ m_e$, which is appropriate to the 2DEG formed in a GaAs/AlGaAs heterostructure, and the Fermi energy of the electrons in the 2DEG regions is set at $E_F = 8.6$ meV.

Most of our calculations presented in this work have been made for the double slit with the slit lengths $L_s = 800$ nm, the radius of the quarter-circle in each slit corner $R_s = 200$ nm, and the slit spacing in the double slit $D_s = 500$ nm. Figure 1(b) shows the calculated conductance of the double slit (without the presence of the single slit in front) as a function of the slit width w_s. Here it is clearly seen that the conductance is quantized in units of $2 \times 2e^2/h$ as expected[1]. In the following, we study the interference patterns of the electrons in the device as shown in figure 1(a) with different numbers of opened modes in the slits. We consider the cases of slit width $w_s = 50$, 75, 100 and 125 nm, corresponding to the cases with one, two, three and four modes opened in the slits, respectively. The single slit for creation of a coherent electron source is placed in a distance of $L_d = 600$ nm from the double slit. The single slit has a length $L_f = 800$ nm and again the radius of the quarter-circle in each slit corner $R_s = 200$ nm. In the quantum conductance regime as studied in this work, the electron wave will pass through the single slit via different lateral modes and therefore show characteristics of the modal structures formed in the slit. As a result, the electron wavefunctions show a lobe or a multi-lobe flow pattern. For interested readers, we include in the appendix the calculated coherent flow patterns for the electrons propagating through the single slit with four different slit widths of $w_f = 50$, 75, 100 and 125 nm, corresponding the cases with one, two, three, and four modes opened in the slit.

Now we study the electron interference patterns of the double-slit device depicted in figure 1(a). We first consider the devices which are symmetric with respect to the x axis. Figure 2 shows the interference patterns of electrons flowing from the double slit in the device with all the three slits having the same width. Figure 2(a) shows the calculated electron density for the device with the slit widths $w_s = w_f = 50$ nm. In this case, only the first mode is open for conduction in each slit. Since the electron flow from a slit in this mode only has one lobe, the electron density seen at sufficiently distant position from the double slit shows the famous Young's double-slit fringe pattern: it has a peak in the middle ($y = 0$) and is symmetric with respect to the middle peak. When the slit widths, w_s and w_f, are changed to 75 nm, both the first and second modes are open for conduction in each slit (cf figure 1(b)). Figure 2(b)

[1] The fine dips or oscillations seen at edges of staircases are due to the formation the longitudinal resonant states in the slits; see, e.g., [24]. These dips or oscillations will disappear when the corners of the slits are made smooth enough. We have in this work used quarter-circles to smooth the slit entrances and exits. As a result, most fine dips or oscillations have been removed, except for those at the edges of staircases. However, these remaining fine dips will not affect our results presented in this work, since we have intentionally chosen those parameters for which the conductance stays at a deep plateau region in which no dips or oscillations are present.

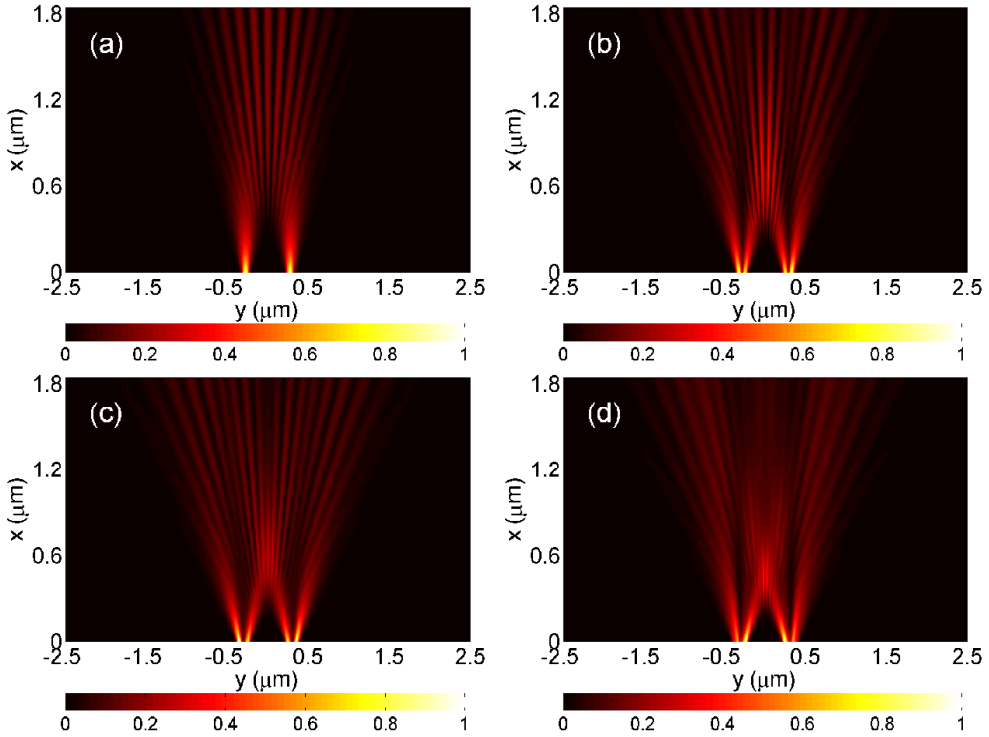

Figure 2. Density plots for electrons at energy $E_F = 8.6$ meV passing through the double-slit device as shown in figure 1(a) with the slit widths of (a) $w_s = w_f = 50$ nm, (b) $w_s = w_f = 75$ nm, (c) $w_s = w_f = 100$ nm, and (d) $w_s = w_f = 125$ nm. The device parameters used in the calculations for these plots are lateral width of the 2DEG regions $W = 5$ μm, slit lengths $L_s = L_f = 800$ nm, slit distance $D_s = 500$ nm, radius of quarter-circles in slit corners $R_s = 200$ nm, and distance between the double slit and the single slit $L_d = 600$ nm. The electron density in each plot has been normalized against its maximum value in the plot.

shows the electron interference pattern for this case. Since the angular pattern of the electron flow from the second mode in a slit has two lobes, the interference pattern seen in figure 2(b) has more complex features. A notable difference from the Young's double-slit interference pattern, as well as from the case for $w_s = w_f = 50$ nm, is that the interference pattern has a dip in the middle. Also the intensity of the fringes seen in figure 2(b) is no longer decreased monotonically from the middle toward the edges. These differences are evidence for the effects of formation of the electron wave modal structure in the slits. When the slit widths, w_s and w_f, are further increased, more and more modes will be opened for conduction in the slits and the electron flow from the double slit generally shows a complex interference structure, as can be seen in figure 2(c) (the case for three modes opened in each slit) or figure 2(d) (the case for four modes opened in each slit). An interesting observation from the results shown in figures 2(a)–(d) is that the interference pattern has a dip in the middle when an even number of modes are opened for conduction in the slits.

Figure 3 shows the interference patterns of electron flow from the double slit in individual modes. As in [4], these interference fringe patterns are obtained from the results for the total electron flow as shown in figures 2(a)–(d) by subtracting the interference patterns for narrower slit cases. For example, to obtain the interference pattern of electron flow only from the

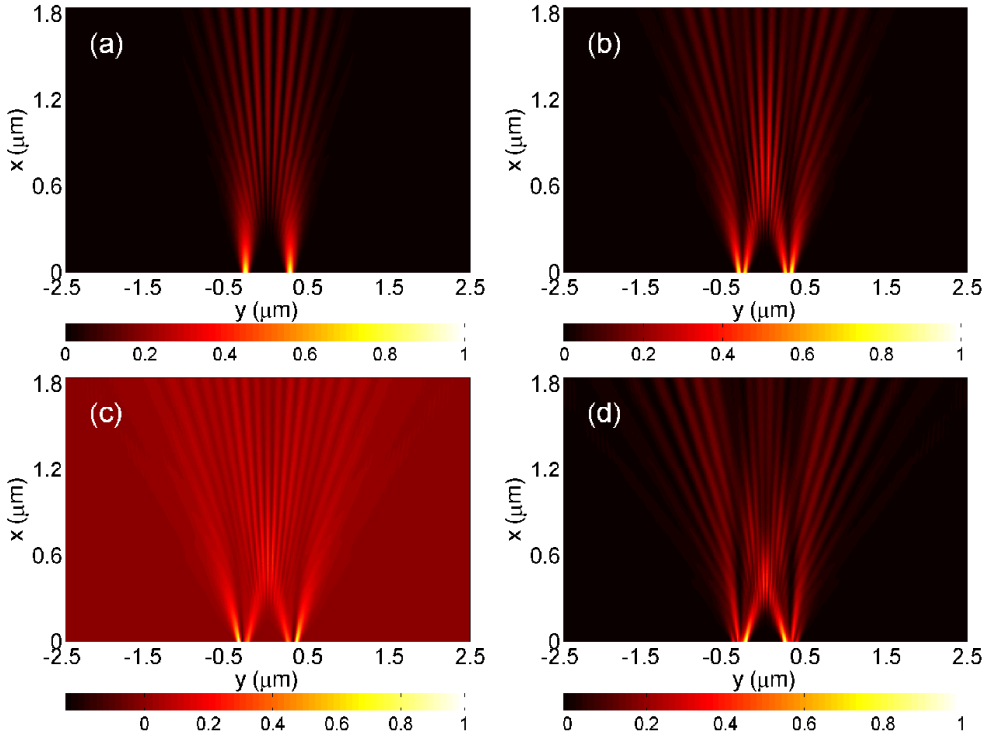

Figure 3. The same as figure 2 but for electron flow from individual modes in the slits. (a) is the same as figure 2(a); (b) is for the density plot for electron flow from the second mode, obtained by subtracting the result in figure 2(a) from the result in figure 2(b); (c) is for the density plot for electron flow from the third mode, obtained by subtracting the result in figure 2(b) from the result in figure 2(c), and finally (d) is for the density plot for electron flow from the fourth mode, obtained by subtracting the result in figure 2(c) from the result in figure 2(d). The electron density in each plot has been normalized against its maximum value in the plot.

third mode as shown in figure 3(c), the total electron flow pattern in figure 2(b) (including the contributions of electron flow from the first and second modes) are subtracted from the total electron flow in figure 2(c) (including the contributions of electron flow from all the first three modes). A comparison with the total electron density plots in figure 2 reveals that the interference pattern of electron flow from the double slit in an individual mode resembles the corresponding interference pattern of the total electron flow well. This result implies that the interference pattern of the total electron flow from the double slit at a given energy is dominated by the interference of electron flow from the highest occupied mode in the slits. The reason for this is as follows. The contribution of each open mode in the double slit to the electron density in the total flow pattern is proportional to $1/k_\alpha$, where k_α is an effective wavenumber of electrons in the double-slit mode α. A higher mode corresponds a smaller value of k_α and thus gives a larger contribution to the electron density in the total electron flow pattern. The comparison also shows that the fringe patterns shown in figure 3 are, in general, sharper than the total flow patterns as shown in figure 2.

As we have discussed above, the single slit introduced in front of the double slit plays an essential role in the observation of sharp interference patterns of electron flow from the double slit. To demonstrate this, we show in figures 4 and 5 the results of calculations for the patterns

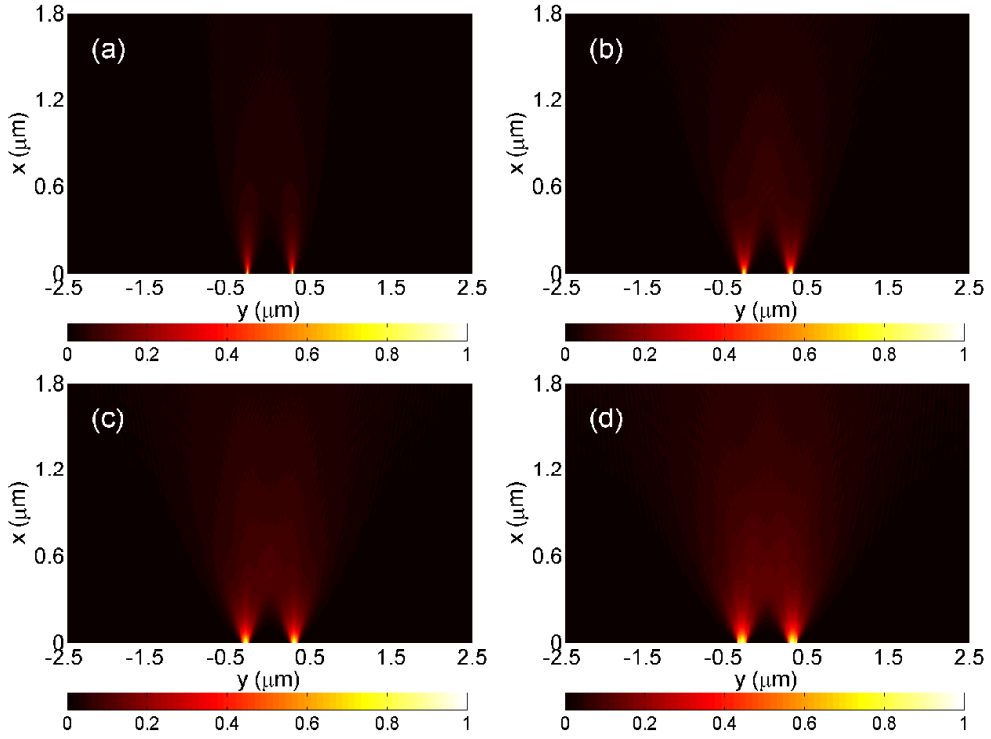

Figure 4. The same as figure 2 but for the density plots for electrons at energy $E_F = 8.6$ meV passing through the double-slit device without presence of the single slit in front. The slit width assumed in the calculation is (a) $w_s = 50$ nm, (b) $w_s = 75$ nm, (c) $w_s = 100$ nm, and (d) $w_s = 125$ nm. The other device parameters assumed are lateral width of the 2DEG regions $W = 5$ μm, slit length $L_s = 800$ nm, slit distance $D_s = 500$ nm, and radius of quarter-circles in slit corners $R_s = 200$ nm. The electron density in each plot has been normalized against its maximum value in the plot.

of electron flow from a pure double slit (i.e., there is no single slit in the left side of the double slit). In these calculations, all the structure parameters used for describing the double slit are the same as in figures 2 and 3. Figures 4(a)–(d) show the total density distributions of electrons for the double slit with the slit widths of $w_s = 50$, 75, 100, and 125 nm, corresponding to the cases with one, two, three and four modes opened in each slit, respectively. It is evident that the total density distributions of electrons flowing from the sole double slit do not show clear interference patterns, in strong contrast to the results of figure 2 where the calculations were made when a single slit was placed in front of the double slit. These results of calculations cast some doubt on the conclusions made from recent hot-electron double-slit interference experiments by Furuya *et al* [20], where no single narrow source of coherent electrons was actually employed in the experiments. Figures 5(a)–(d) show the patterns of the electron flow from the double slit through individual modes in the slits, obtained in the same way as in figures 3(a)–(d) by the subtraction procedure. Although weak, blurred, wide fringes are visible in the density distribution patterns of electrons flowing from the double slit through high index individual modes, the sharp, fine interference fringe patterns as found in figure 3 are completely invisible in figure 5. Thus, employment of a single slit in front of the double slit is essential for observation of a fine interference fringe pattern in Young's double-slit experiments for electrons.

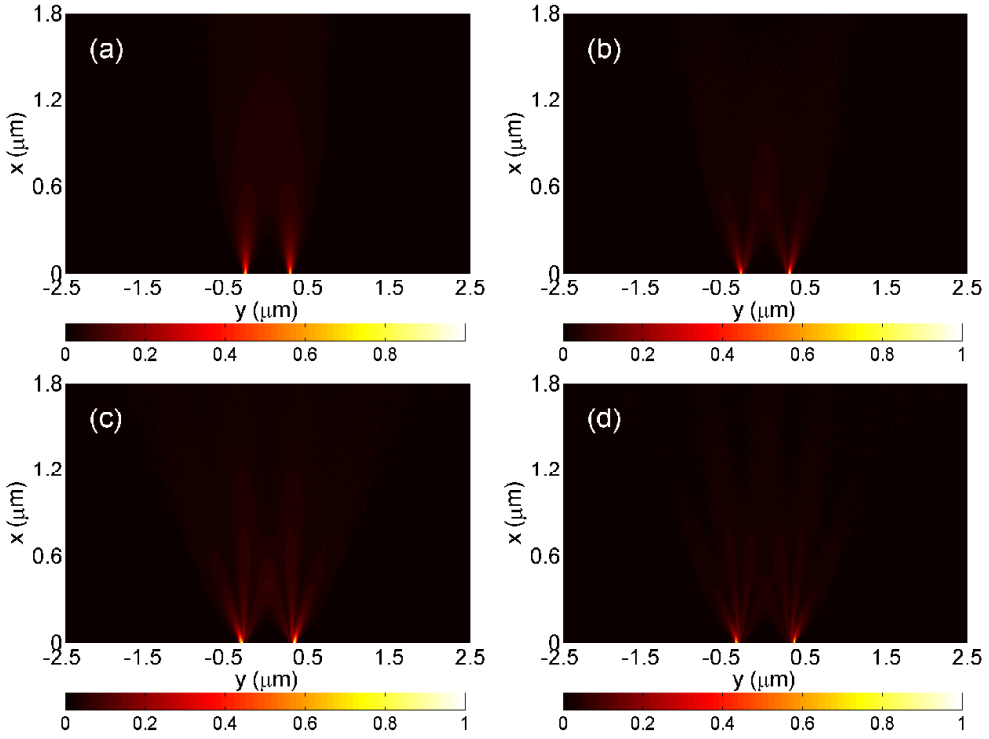

Figure 5. The same as figure 3 but for electron flow from individual modes in the same pure double-slit structure as in figure 4. The electron density in each plot has been normalized against its maximum value in the plot.

Because the role of the single slit placed in front of the double slit is to create a source of coherent electrons incident on the double slit with similar initial conditions, the narrower the employed single slit, the sharper the interference fringes of the double slit. However, due to the wave nature of electrons, it is impossible to make the single slit infinitely narrow in width. Figures 6 and 7 show the interference patterns of electrons flowing from the double slit for two different widths of the single slit. Clearly, similar fine interference patterns as seen in figure 2 are found in both cases. The interference fringes are, however, found to be very different in sharpness in the two cases: the fringe pattern is much sharper in the case where the width of the front single slit is set at $w_f = 50$ nm (figure 6) than in the case where the width of the front single slit is set at $w_f = 125$ nm (figure 7). The difference can be explained as follows. At the width of $w_f = 125$ nm, electrons with energy $E_F = 8.6$ meV can propagate through the front single slit through its four lowest modes (see the appendix). The interference patterns of the double slit for electrons propagating through different single-slit modes are independent and are, in general, different. Thus, the interference patterns found in figure 7 are the results of a superposition of the four individual contributions and are therefore blurred. However, at $w_f = 50$ nm, only the lowest single-slit mode is open for the electron transmission at energy $E_F = 8.6$ meV. Thus the interference pattern of the double slit in figure 6 contains the sole contribution from electrons that pass through the front single slit through its lowest mode.

It is seen, in figures 2, 3, 6, and 7, that the electron flow patterns are very different in the regions with different distances from the double slit. For a better description of the electron flow

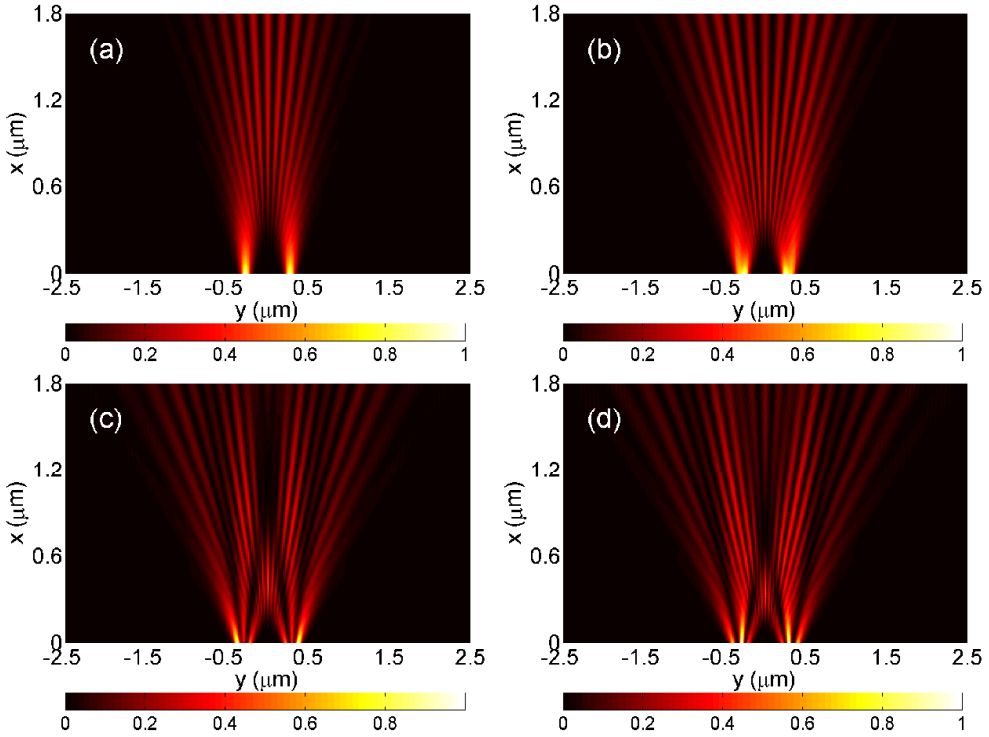

Figure 6. Density plots for electrons at energy $E_F = 8.6$ meV passing through the same double-slit device as in figure 2 but for the width of the front single slit fixed at $w_f = 50$ nm. The slit width in the double slit is (a) $w_s = 50$ nm, (b) $w_s = 75$ nm, (c) $w_s = 100$ nm, and (d) $w_s = 125$ nm. The other device parameters used in the calculations are the same as in figure 2 with $W = 5$ μm, $L_s = L_f = 800$ nm, $D_s = 500$ nm, $R_s = 200$ nm, and $L_d = 600$ nm. The electron density in each plot has been normalized against its maximum value in the plot.

characteristics in different regions, we have made line plots for the electron density distributions along the transverse direction at some selected detection positions. As an example, we show in figure 8 the plots for the electron density distributions at four selected detection positions for the patterns of the electron flow from individual modes as shown in figure 3. It is evident that at a large value of x (the far-field regime), only the interference pattern for the case of electron flow through the first mode in the double slit shows the regular, Young's double-slit interference pattern (figure 8(a)). The far-field interference patterns for the cases of electron flow from higher modes in the double slit show complex interference structures. Note that the very fast regular oscillations seen in the electron density distributions at large values of x (figures 8(b)–(d)) arise from the finite lateral size ($W = 5$ μm) of the 2DEG region assumed in the calculations. These oscillations gradually disappear when the lateral size W is further increased. At $x = 500$ nm (a value in the near-field regime), the envelopes of the oscillated electron density distributions show rather regular patterns: the envelope shows a double-peak structure in the case of electron flow from the first mode in the double slit and a triple-peak structure in the case of electron flow from a high index mode in the double slit. The electron flow tends to focus on the central region in the near-field regime. In particular, a strong electron density envelope peak is found in the central region in the case of electron flow from the second, third, or fourth mode in the double slit (see figures 8(b)–(d)).

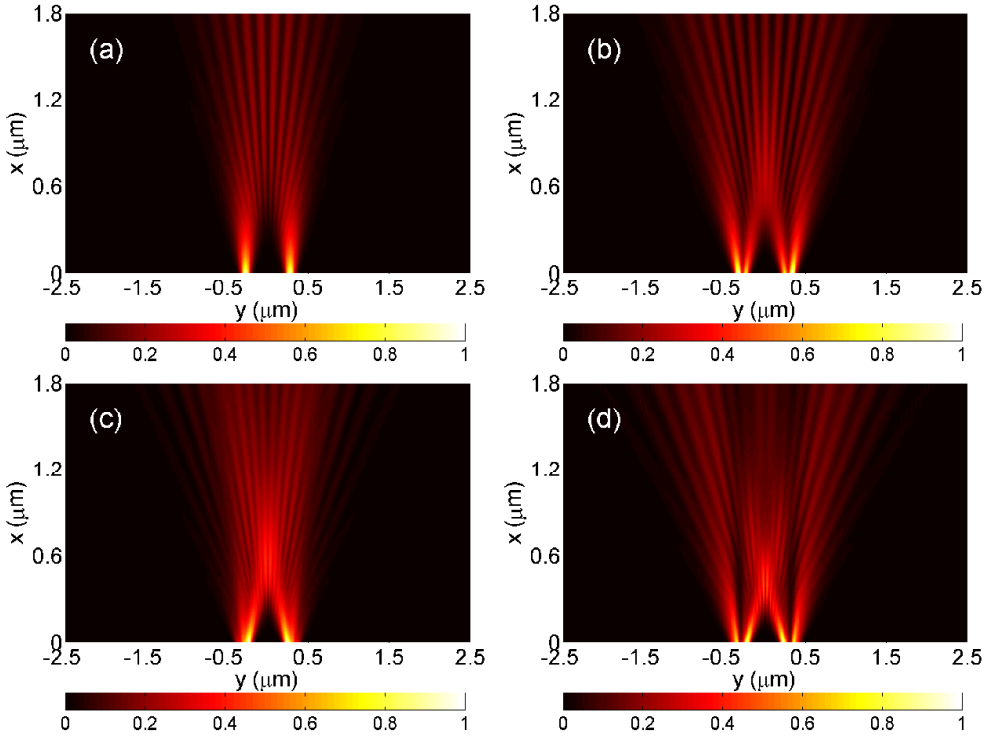

Figure 7. The same as figure 6 but for the width of the front single slit fixed at $w_f = 125$ nm. Also, as in figure 6, the electron density in each plot has been normalized against its maximum value in the plot.

In the results we have presented above, the single slit in front of the double slit has been placed in such a way that the complete double-slit device is symmetric under reflection with respect to the x axis. In experiments, it is hard to fabricate such a completely symmetric system. Therefore it is interesting to know how the interference effects are influenced by symmetry breaking in the system. In the following, we discuss, as an example, only the case when the system symmetry is broken by misalignment of the single slit with respect to the central line of the double slit (the x axis). Figure 9 shows the total density distributions of electrons flowing from the same double-slit structure as in figure 2, but with a shift of the single slit along the y direction by 50 nm. In this asymmetric device, the patterns of electron flow from the double slit still show clear interference fringes and resemble the results presented in figure 2 well. However, due to the breaking of reflection symmetry of the system, the wavefunction for an electron flowing from the double slit is no longer symmetric or antisymmetric with respect to the x axis ($y = 0$). Thus the interference fringe patterns of electron flow from the double slit as shown in figure 9 do not have reflection symmetry. This is particularly clear in the cases of electron flow from high index modes in the double slit (see figures 9(b)–(d)).

Finally, we study the dependence of the spacing of the interference fringes on the slit distance D_s in the double slit (cf figure 1(a)). Figures 10(a) and (b) show the centre-to-centre spatial separation, d, of adjacent fringes in the middle region of the interference patterns as a function of D_s for the device as shown in figure 1(a) with the same structure parameters as in figures 2(a) and (d) except for the varying slit distance D_s. Note that in these calculations, the radius of the quarter-circle, R_s, used to smooth each slit corner is varied with varying D_s

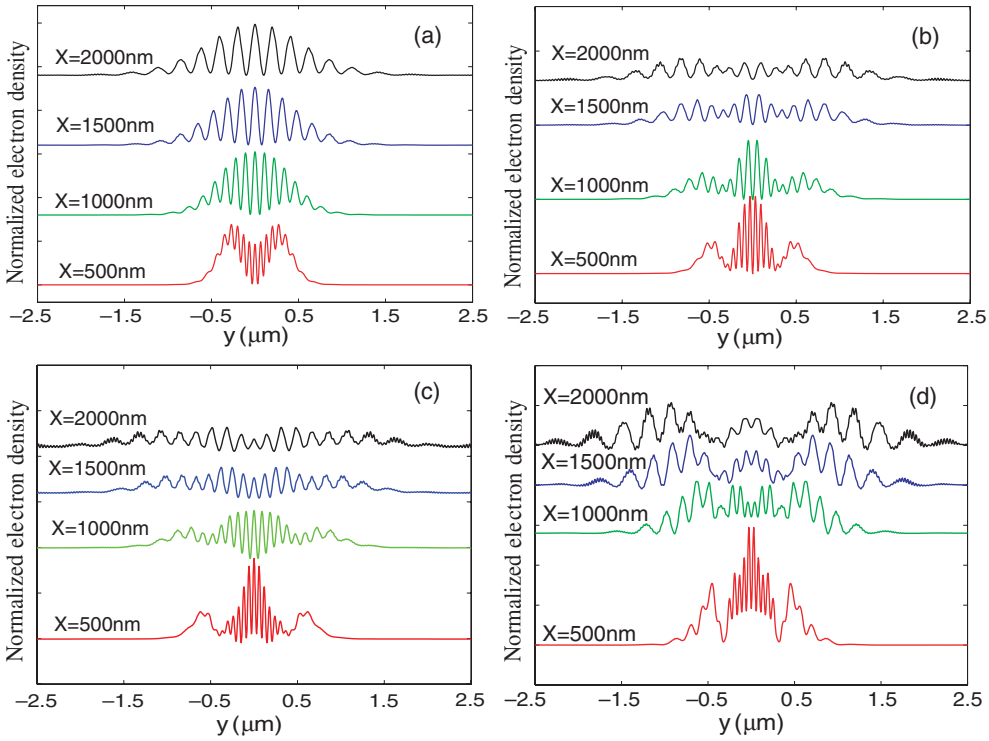

Figure 8. The same normalized electron densities for electron flow from (a) the first mode, (b) the second mode, (c) the third mode, and (d) the fourth mode as in figure 3, but being plotted at four selected detection distances (x values) from the double slit.

according to $R_s = (D_s/2) - 50$ nm and the slit lengths are varied as $L_s = L_f = R_s + 400$ nm. Note also that in figure 2(a), the wavefunctions of electrons have an even parity and the interference pattern of the double slit has a bright fringe at $y = 0$. The spatial separation, d, in this case is taken as the centre-to-centre distance of the bright fringe at $y = 0$ and one of its neighbouring bright fringes. The results in figure 10 show that with increasing D_s, the spatial separation of bright fringes, d, deceases as expected. However, in general, it is difficult to extract a simple relation between the fringe spacing d and the slit distance D_s. This is particularly true in the case with a large slit width for which the electron flow from the double slit shows a complicate interference pattern due to the presence of a multi-lobe structure in the flow from each slit. Nevertheless, we were able to conclude that in the near-field regime (e.g., at $x = 500$ nm), the fringe spacing d of the interference pattern changes slowly with varying D_s when compared with the results found in the far-field regime (see, e.g., the case at $x = 2000$ nm).

4. Conclusions

In summary, we have theoretically studied the quantum interference behaviour of electron flow from a double-slit device made from a semiconductor 2DEG system with the slit widths in the quantum conductance regime. The device consists of a double slit and a single slit in a configuration where the single slit is placed on the electron source side of the double slit. On the basis of a scattering matrix method, the wavefunctions of electrons passing through

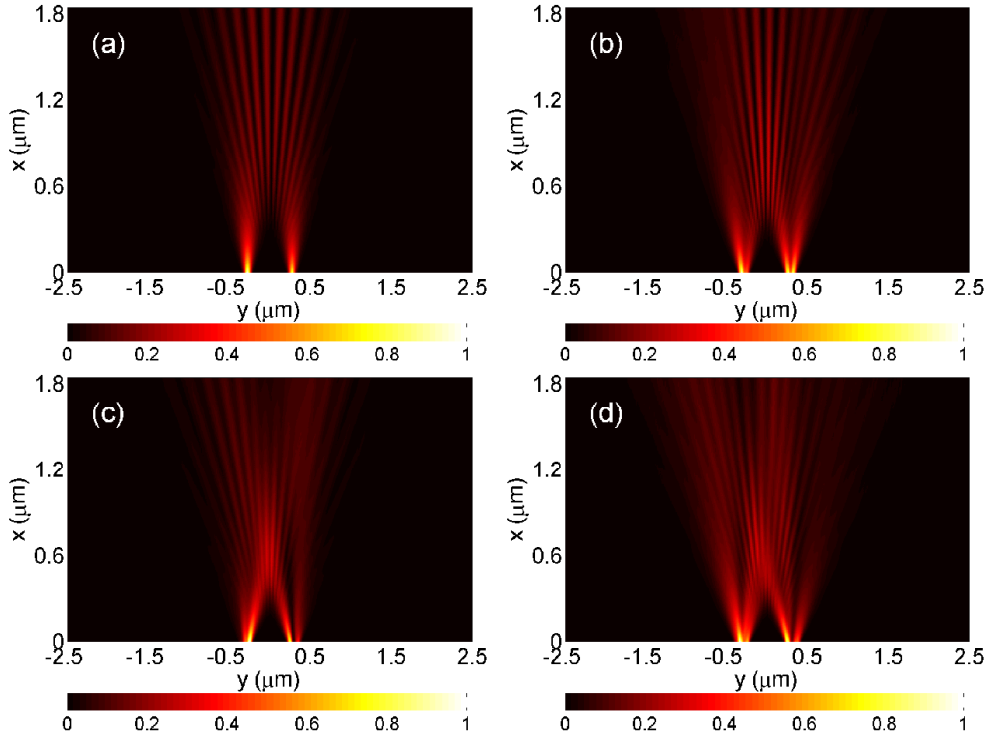

Figure 9. Density plots for electrons at energy $E_F = 8.6$ meV passing through the double-slit device with the slit widths of (a) $w_s = w_f = 50$ nm, (b) $w_s = w_f = 75$ nm, (c) $w_s = w_f = 100$ nm, and (d) $w_s = w_f = 125$ nm. The device parameters used in the calculations for these plots are the same as in figure 2 except that the position of the single slit has been shifted by 50 nm along the y direction. The electron density in each plot has been normalized against its maximum value in the plot.

the double-slit structure are calculated. It is found that including a single slit between the double slit and the source contact in the device is essential for the observation of interference fringes of electron flow in a double-slit experiment with a 2DEG. When only the lowest mode is open for conduction in the three individual slits, the interference patterns of electron flow from the double slit resemble the results of a conventional Young's double-slit experiment well. When several modes are open for conduction in the individual slits, the interference patterns of electron flow from the double slit are dominated by the interference of electrons flowing through the highest open modes in the slits and, in general, show rather complex structures. The characteristics of the interference patterns in the near- and far-field regimes have also been discussed, as well as the dependence of the fringe spacing on the slit distance in the double slit. In general, the fringe spacing decreases as the slit distance in the double slit increases. However, it is difficult to extract a simple relation between the fringe spacing and the slit distance, due to presence of lobe structures in the electron flow from the slits in the quantum conductance regime. Clearly, it is interesting to extend our calculations to include scattering in the 2DEG region on the collector side of the double slit and to study interference phenomena from branched strands in the electron flow from the double slit. Another direction of interest is including spin–orbit interaction in the calculations using the formalism recently reported in [25] and studying its effect on interference patterns from the double slit. We expect

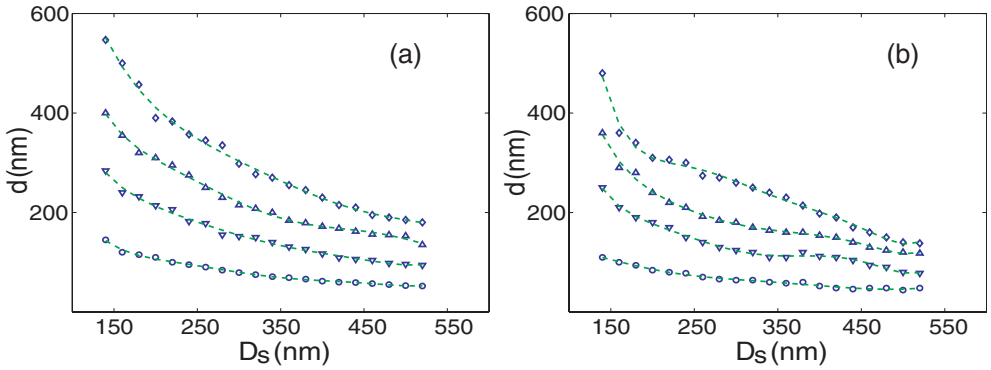

Figure 10. Centre-to-centre spatial separation, d, of adjacent fringes in the middle region of the interference pattern as a function of the slit distance D_s for the device as in figure 2 with (a) the slit widths $w_s = w_f = 50$ nm and (b) the slit widths $w_s = w_f = 125$ nm. The other device parameters used in the calculations are the same as in figure 2. In each figure, we plot the spatial separation d versus the slit distance D_s, calculated at $x = 500$ nm (circle), 1000 nm (down-triangle), 1500 nm (up-triangle) and 2000 nm (diamond). The marks are the calculations, while the dashed lines are polynomial fits to the data as guides for the eyes.

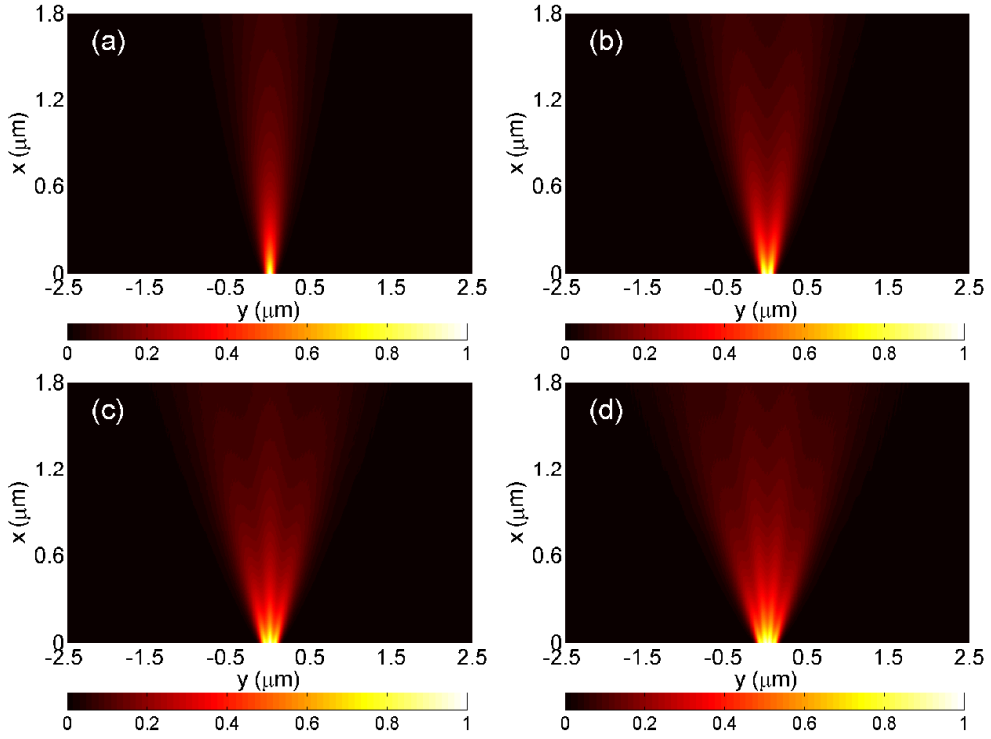

Figure A.1. Density plots for electrons at energy $E_F = 8.6$ meV passing through a pure single slit, which is the same as the one placed in front of the double slit in figure 1(a), with the slit width of (a) $w_f = 50$ nm, (b) $w_f = 75$ nm, (c) $w_f = 100$ nm, and (d) $w_f = 125$ nm. The other device parameters used in the calculations for these plots are lateral width of the 2DEG regions $W = 5$ μm, slit length $L_f = 800$ nm, and radius of quarter-circles in slit corners $R_s = 200$ nm. The electron density in each plot has been normalized against its maximum value in the plot.

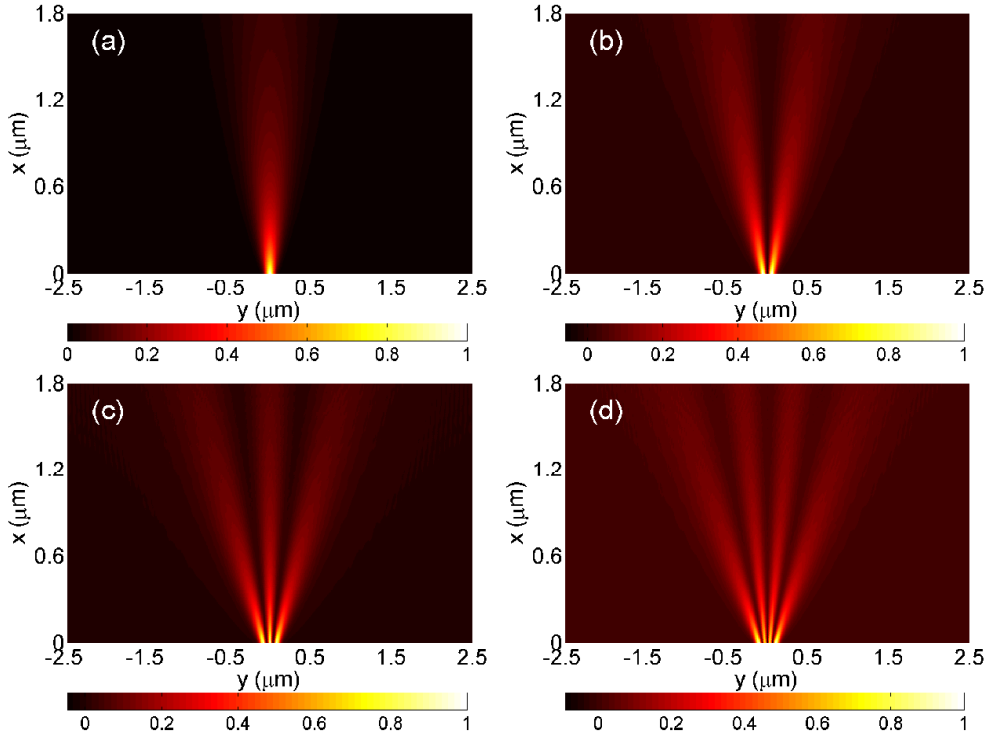

Figure A.2. The same as figure A.1 but for electron flow from the single slit through (a) the first slit mode, (b) the second slit mode, (c) the third slit mode, and (d) the fourth slit mode, obtained in the same way as in figure 3 by a subtraction procedure. The electron density in each plot has been normalized against its maximum value in the plot.

that our work will stimulate experimental efforts on the observation of interference phenomena of electron flow from a double slit made from a semiconductor 2DEG system.

Acknowledgments

This work was supported by the Swedish Research Council (VR) and the Swedish Foundation for Strategic Research (SSF) through the Nanometre Structure Consortium at Lund University.

Appendix

The front single slit in the double-slit device as shown in figure 1(a) plays an important role in generating a high quality, sharp interference fringe pattern of the double slit. However, in the quantum conductance regime, the electrons passing through the single slit show the characteristics of the modal structures formed in the slit [4–6]. Namely, the electron wave propagating through the single slit via a quantum mode does not emit from the opening with a spatially uniform wave intensity profile, in contrast to what is described in classical wave mechanics. For completeness and to give a general reader a better understanding of the effects of a single slit in a double-slit experiment, we show in figures A.1 and A.2 the flow patterns of the electrons passing through a single slit with different widths. Figure A.1 shows the density

plots for electrons at energy $E_F = 8.6$ meV passing through the same single slit as was shown in figure 1(a) with widths of $w_f = 50$, 75, 100, and 125 nm, corresponding to the situations where one, two, three, and four modes are open for the electron transmission in the slit. It is seen that for the slit with the width $w_f = 50$ nm, the electron flow pattern is characterized by a broad lobe. When the width of the single slit is increased to 75, 100, and 125 nm, weak multi-lobe structures are visible in the density plots and the number of lobes seen in an electron flow pattern is equal to the number of open modes in the slit. The multi-lobe electron flow structures are more clearly seen in figure A.2, where the electron flows from the slit through individual modes, obtained in the same way as for figure 3 by a subtraction procedure, are plotted.

References

[1] Jönsson C 1974 *Am. J. Phys.* **42** 4
[2] Merli P G, Missiroli G F and Pozzi G 1976 *Am. J. Phys.* **44** 306
[3] Tonomura A, Endo J, Matsuda T, Kawasaki T and Ezawa H 1989 *Am. J. Phys.* **57** 117
[4] Topinka M A, LeRoy B J, Shaw S E J, Heller E J, Westervelt R M, Maranowski K D and Gossard A C 2000 *Science* **289** 2323
[5] Topinka M A, Westervelt R M and Heller E J 2003 *Phys. Today* **56** 47
[6] LeRoy B J 2003 *J. Phys.: Condens. Matter* **15** R1835
[7] Topinka M A, LeRoy B J, Westervelt R M, Shaw S E J, Fleischmann R, Heller E J, Maranowski K D and Gossard A C 2001 *Nature* **410** 183
[8] Yoo M J, Fulton T A, Hess H F, Willett R L, Dunkleberger L N, Chichester R J, Pfeiffer L N and West K W 1997 *Science* **276** 579
[9] Tessmer S H, Glicofridis P I, Ashoori R C, Levitov L S and Melloch M R 1998 *Nature* **392** 51
Chakraborty S, Maasilta I J, Tessmer S H and Melloch M R 2004 *Phys. Rev.* B **69** 073308
[10] Venema L C, Wildöer J W G, Janssen J W, Tans S J, Tuinstra H L J T, Kouwenhoven L P and Dekker C 1999 *Science* **283** 52
[11] Lemay S G, Janssen J W, van den Hout M, Mooij M, Bronikowski M J, Willis P A, Smalley R E, Kouwenhoven L P and Dekker C 2001 *Nature* **412** 617
[12] Woodside M T and McEuen P L 2002 *Science* **296** 1098
[13] Zhitenev N B, Fulton T A, Yacoby A, Hess H F, Pfeiffer L N and West K W 2000 *Nature* **404** 473
[14] Morgenstern M, Klijn J, Meyer C, Getzlaff M, Adelung R, Römer R A, Rossnagel K, Kipp L, Skibowski M and Wiesendanger R 2002 *Phys. Rev. Lett.* **89** 136806
[15] Morgenstern M, Klijn J, Meyer C and Wiesendanger R 2003 *Phys. Rev. Lett.* **90** 056804
[16] Crook R, Smith C G, Graham A C, Farrer I, Beere H E and Ritchie D A 2003 *Phys. Rev. Lett.* **91** 246803
[17] Aoki N, da Cunha C R, Akis R, Ferry D K and Ochiai Y 2005 *Appl. Phys. Lett.* **87** 223501
Aoki N, da Cunha C R, Akis R, Ferry D K and Ochiai Y 2005 *Phys. Rev.* B **72** 155327
[18] Steele G A, Ashoori R C, Pfeiffer L N and West K W 2005 *Phys. Rev. Lett.* **95** 136804
[19] LeRoy B J, Bleszynski A C, Aidala K E, Westervelt R M, Kalben A, Heller E J, Shaw S E J, Maranowski K D and Gossard A C 2005 *Phys. Rev. Lett.* **94** 126801
[20] Furuya K, Ninomiya Y, Machida N and Miyamoto Y 2003 *Phys. Rev. Lett.* **91** 216803
[21] Ko D Y K and Inkon J C 1988 *Phys. Rev.* B **38** 9945
[22] Xu H 1994 *Phys. Rev.* B **50** 8469
Xu H 1995 *Phys. Rev.* B **52** 5803
[23] Xu H 1993 *Phys. Rev.* B **47** 9537
[24] Kirczenow G 1989 *Phys. Rev.* B **39** 10452
Xu H 1993 *Phys. Rev.* B **47** 15630
[25] Zhang L, Brusheim P and Xu H Q 2005 *Phys. Rev.* B **72** 045347